Theor Chem Acc (2016) 135:218
DOI 10.1007/s00214-016-1943-4

REGULAR ARTICLE

Theoretical elucidation of the metabolic mechanisms of phenothiazine neuroleptic chlorpromazine catalyzed by cytochrome P450 isoenzyme 1A2

Zhiyu Xue[1,2] · Yan Zhang[1,2] · Jing Tao[1] · Yuan Kang[1] · Zeqin Chen[1] · Ying Xue[2]

Received: 2 November 2015 / Accepted: 5 July 2016 / Published online: 13 August 2016

Abstract Chlorpromazine, belonging to the first-generation antipsychotics, is known to cause some side effects, such as hepatotoxicity and agranulocytosis. The metabolic mechanisms of chlorpromazine remain elusive up to now, but are thought to result in the formation of some reactive metabolites having side effects on the parent drug. The goal of this work was to explore the metabolic mechanisms of chlorpromazine catalyzed by cytochrome P450 isoenzyme 1A2, a highly important activating enzyme of cytochrome P450 family, using DFT calculation. Three types of metabolic mechanisms were characterized, including S-oxidation, aromatic hydroxylation and *N*-dealkylation. The calculated results demonstrate that N_{14}-demethylation is the most thermodynamically and kinetically favorable metabolic pathway of chlorpromazine, followed by S_5-oxidation. Then, mono-*N*-desmethylchlorpromazine is the most feasible chlorpromazine metabolite, which can occur further demethylation to form di-*N*-desmethylchlorpromazine. Besides, chlorpromazine 5-sulfoxide and 7-hydroxychlorpromazine are both the possible metabolites of chlorpromazine. Interestingly, *N*-methyl hydroxylation, the rate-limiting step of *N*-demethylation, proceeds predominantly via a single-electron-transfer mechanism. All the proton transfer processes involved in the aromatic hydroxylation and *N*-dealkylation prefer to occurrence in a water-assisted enzymatic process. Each metabolic pathway proceeds in the spin-selective manner via the low-spin state of Cpd I. Our results are in good accordance with the experimental observations, which can provide some essential implications for the metabolic mechanisms of chlorpromazine-like drugs.

Keywords Chlorpromazine · CYP1A2 · S-oxidation · Aromatic hydroxylation · *N*-dealkylation

1 Introduction

Chlorpromazine, a member of phenothiazine neuroleptics of an aliphatic type, belongs to the first generation of antipsychotics. Acting as a strong antagonist of the dopaminergic D_2 receptor, chlorpromazine exhibits the antipsychotic effect and wide application in the treatment of schizophrenia, psychotic disorders and manic phase of bipolar disorders [1–4], which, however, is associated with the extrapyramidal side effect of chlorpromazine [5, 6]. Besides, the prolonged periods or high dosages (>2 g/day) of chlorpromazine may also cause skin disorders, ocular effects and rare, but severe irreversible corneal edema if not promptly identified [7–11].

Chlorpromazine clearance is an enzymatic process and occurs extensively in the liver. Cytochrome P450 (CYP), an important heme-containing enzyme superfamily existing in multiple and distinct isoenzymes, is potentially

Zhiyu Xue and Yan Zhang authors have contributed equally to this work.

Electronic supplementary material The online version of this article (doi:10.1007/s00214-016-1943-4) contains supplementary material, which is available to authorized users.

✉ Zeqin Chen
chenzeqin@cwnu.edu.cn

[1] College of Chemistry and Chemical Engineering, Chemical Synthesis and Pollution Control Key Laboratory of Sichuan Province, China West Normal University, Nanchong 637002, People's Republic of China

[2] College of Chemistry, Key Laboratory of Green Chemistry and Technology in Ministry of Education, Sichuan University, Chengdu 610064, People's Republic of China

responsible for the metabolism of chlorpromazine [12]. The biotransformation of chlorpromazine mainly proceeds via *N*-dealkylation, S-oxidation and aromatic hydroxylation, which result in the formation of different metabolites, including mono-*N*-desmethylchlorpromazine, di-*N*-desmethylchlorpromazine, chlorpromazine 5-sulfoxide, 7-hydroxychlorpromazine and 8-hydroxychlorpromazine (Scheme 1). Binding studies have shown that 7-hydroxychlorpromazine and mono-*N*-desmethylchlorpromazine are the most active metabolites of chlorpromazine [13], which own approximately 50 % of the parent compound activity in blocking D_2 and a_1 receptors. Besides, high levels of chlorpromazine 5-sulfoxide seem to have a side effect on therapeutic response in schizophrenic patients. All these metabolites are weak antagonists of the M_1 receptor [14, 15]. Hence, most of the metabolites exhibit biological activity and may contribute to the side effects of the parent drug [16, 17].

To date, many studies have devoted to find out the particular metabolic processes of chlorpromazine for which different cytochrome P450 isoenzymes are responsible. A recent study on cDNA-expressed human CYP isoenzymes showed that hepatic CYP1A2 is the only CYP isoenzyme that catalyzes the mono-*N*-demethylation and di-N-demethylation of chlorpromazine and is the main isoenzyme responsible for chlorpromazine 5-sulfoxidation at a therapeutic concentrations of the drug. CYP3A4 contributes to chlorpromazine 5-sulfoxidation to a lesser extent [12]. The catalysis of chlorpromazine *N*-demethylation and 5-sulfoxidation in humans exhibits a stricter CYP1A2 preference compared with the previously tested perazine, promazine and thioridazine [18–20]. On the other hand, cigarette smoking has been reported to increase the clearance of chlorpromazine [21]. Cigarette smoking is well known to cause marked induction of CYP1A2 and accelerate the metabolism of drugs catalyzed by CYP1A2, such as

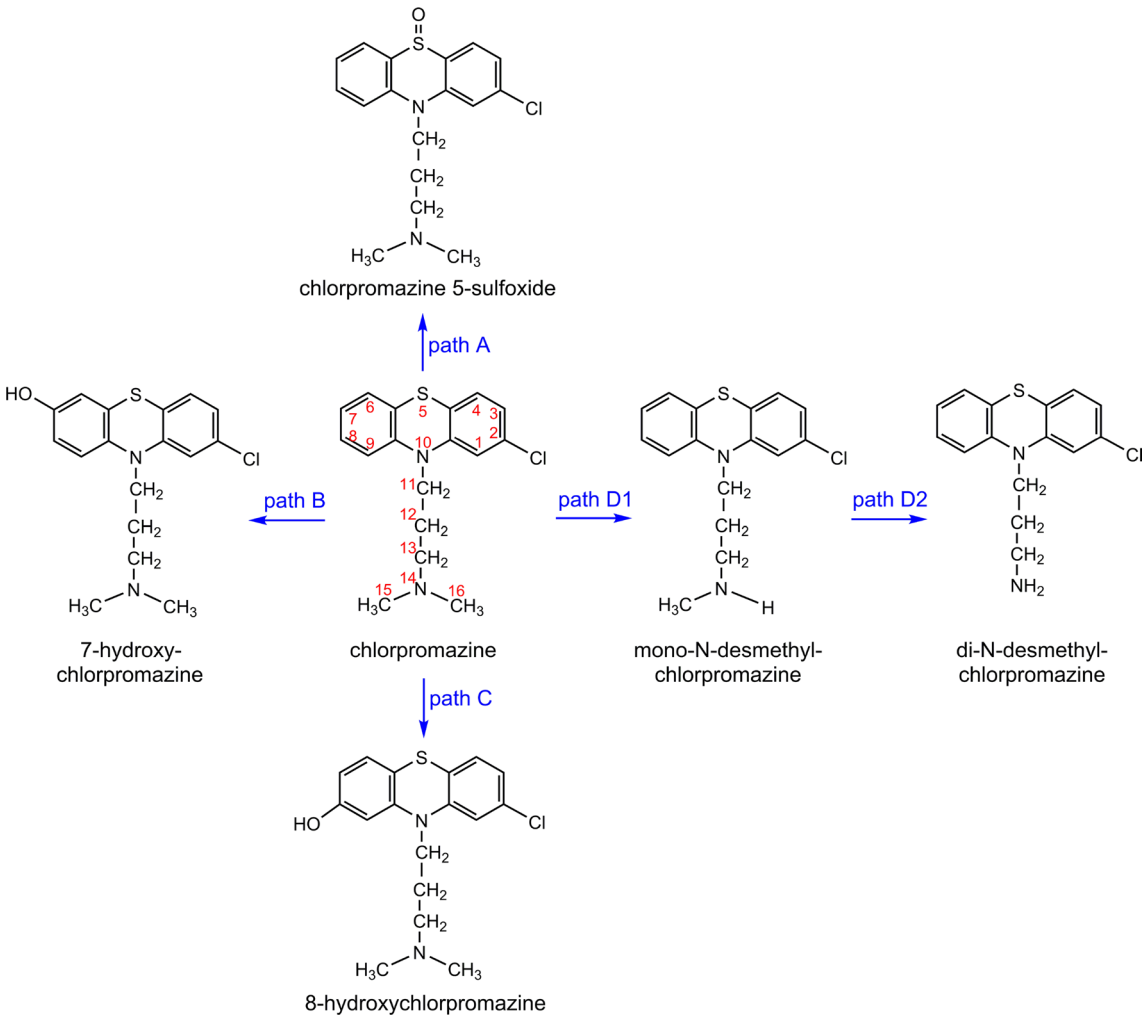

Scheme 1 Possible metabolic pathways of chlorpromazine catalyzed by CYP1A2

theobromine and caffeine [22]. Consequently, CYP1A2 is significantly involved in the metabolism of chlorpromazine.

The complete depiction of the metabolic mechanisms of chlorpromazine by CYP1A2 is presented in Scheme 2. The active species of CYP1A2 in catalysis is believed to be a $Fe^{IV} = O$ complex with a porphyrin radical, referred to as compound I (Cpd I in brief) [23]. Originating from the high-spin (HS) quartet and low-spin (LS) doublet states of Cpd I, theoretical studies have suggested two possible mechanisms: the spin-selective manner (SSM) scenario and the two-state reactivity (TSR) [24]. For *N*-methyl hydroxylation, the first step of *N*-demethylation, two controversial mechanisms, single electron transfer (SET) [25, 26] versus hydrogen atom transfer (HAT) (Scheme 2) [27, 28], have existed for decades. There are not any standard rules to generalize their application, since the preferred mechanism is dependent on the detailed characteristics of the amine [29]. Our previous study on the caffeine metabolism catalyzed by CYP1A2 revealed a HAT mechanism with the TSR mechanism [30]. As of yet, the mechanic details of chlorpromazine metabolism catalyzed by CYP1A2 are still unclear. Some intriguing puzzles still remain, on which theory can provide the undiscovered insight and reveal some new features, such as, which mechanism does chlorpromazine metabolism favor: TSR or SSM? Which kind of mechanism does chlorpromazine *N*-demethylation proceed by: HAT or SET? Why chlorpromazine 8-hydroxylation is not mentioned in the previous experiments though the C_7 and C_8 atoms of chlorpromazine have similar characteristic? Which metabolic pathway predominates?

The present work aimed to clarify the aforementioned puzzles to resolve the mechanistic details of chlorpromazine by CYP1A2 using density functional theoretical (DFT) calculations. This observation can provide some essential clues for the pharmacological study.

2 Methodology

With the purpose of gaining a theoretical insight into the vital metabolic mechanism of chlorpromazine catalyzed by CYP1A2, a popular six-coordinate oxo-ferryl species model, $Fe^{4+}O^{2-}(C_{20}N_4H_{12})^{-}(SH)^{-}$ [31], was employed as the reactive Cpd I of CYP1A2, which contains a truncated

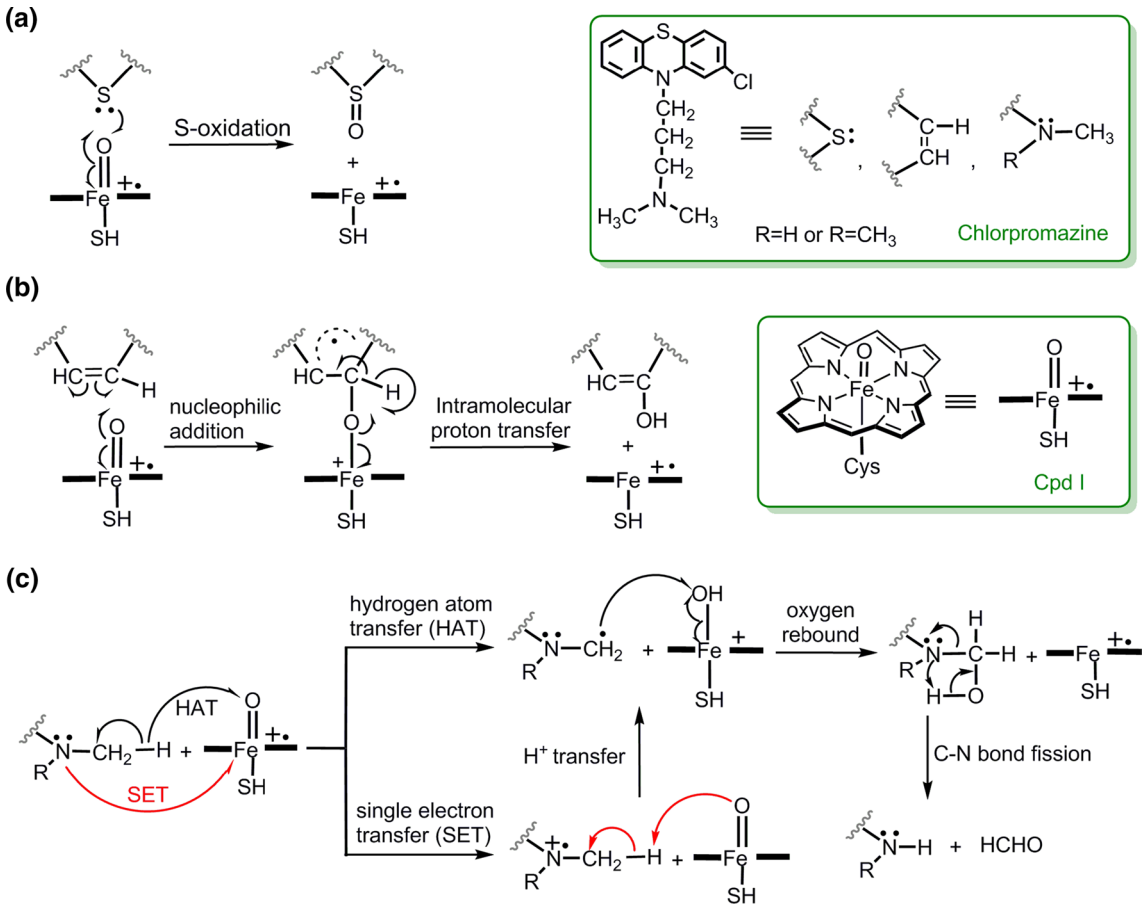

Scheme 2 Metabolic mechanisms of chlorpromazine catalyzed by CYP1A2. **a** S-oxidation, **b** aromatic hydroxylation and **c** *N*-demethylation

heme and a thiolate axial ligand (SH–) built from the crystal structure of CYP1A2 (PDB:2HI4) [32]. The spin-unrestricted B3LYP was adopted with two basis sets: (a) LACVP(Fe)/6-31G (H, C, N, O, S, Cl) (B1 in brief) for the optimization of all the stationary points without symmetry constraints and (b) LACV3P+*(Fe)/6-311++G(d,p) (the rest) (B2 in brief) for single-point energy calculation both in the gas phase and in the protein environment to obtain reliable energetics. These model and computational methods chosen have been tested extensively and proven to be reliable in solving cytochrome P450 enzymes problems [23, 30, 33–37]. Transition states were affirmed by harmonic frequency analysis to possess only one imaginary frequency, and the stationary points were confirmed as minima with all positive frequencies. The validity of the TS geometry was verified by intrinsic reaction coordinate (IRC) calculations [38]. Natural population atomic (NPA) charges were determined using Reed and Weinhold's natural bond orbital (NBO) analysis [39]. The binding energies of substrates to heme were corrected using basis set superposition error.

The weak polarization effect of the protein environment was modeled using PCM solvation method [40] with the dielectric constant of $\varepsilon = 5.62$ (chlorobenzene), which was taken as a reasonable compromise for the enzyme active site [41]. All of the single-point energies in chlorobenzene were corrected by the gas-phase thermodynamic quantities. The thermodynamic data reported in this paper are at 298.15 K and 1 atm. Cartesian coordinates for all the optimized geometries are presented in Supporting Information (SI) section. All DFT calculations were done using Gaussian 09 suite of programs [42].

3 Results and discussion

During phase I of metabolism, five possible catalytic pathways of CYP1A2 to chlorpromazine were investigated (Scheme 1), including oxidation at the S_5 site of the thiazine ring (S_5-oxidation, path A), aromatic hydroxylations at C_7 (C_7-hydroxylation, path B) and C_8 (C_8-hydroxylation, path C) sites as well as mono-*N*-demethylation (path D1) and di-*N*-demethylation (path D2) at N_{14} site. The complete reaction mechanisms of S-oxidation, C-hydroxylation and *N*-demethylation are depicted in Scheme 2. Each pathway is discussed in detail below.

3.1 S_5-oxidation (path A)

Path A is a one-step reaction, which involves the direct oxidation of S_5 atom by Cpd I (Scheme 2a). The optimized geometries of all the stationary points are presented in Fig. 1. The located transition-state A-TS_1 species, A-$^2TS_1$ and A-$^4TS_1$, is characterized by its single imaginary frequency of 219.7i cm^{-1} LS and 601.9i cm^{-1} HS. It implies that heavy oxygen atom motion is comprised in the reaction vector, since, in principle, the magnitude of the imaginary frequency is quite high to exceed 1000 i cm^{-1} if atom motion in the transition state is largely comprised of light hydrogen atom migration [43]. Animation of the single imaginary frequency of A-TS_1 species shows the motion of oxygen atom from Fe to S_5 atoms, leading to Fe–O breakage and S–O bond formation. The Fe–O bond in transition-state A-TS_1 species is elongated by 0.083 Å LS and 0.179 Å HS with respect to their corresponding reactant complex A-RC species, A-^{2}RC and A-^{4}RC. This is companied with

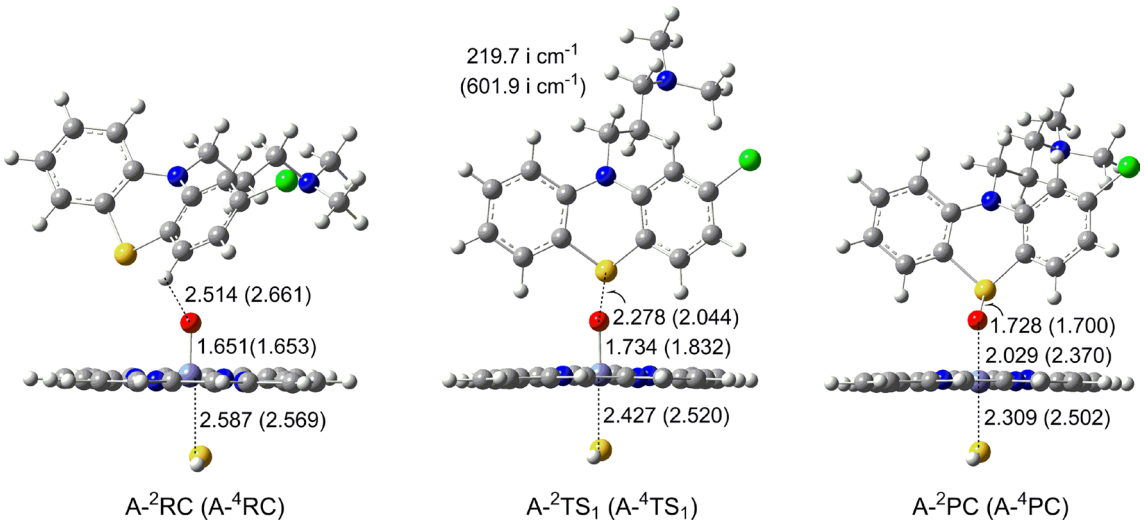

Fig. 1 Optimized structures (in Å) for S_5-oxidation (path A) of chlorpromazine by Cpd I at the B1 level (values out of parentheses, data for LS state; values in parentheses, data for HS state. Definitions are the same in the following structure figures)

the remarkable curtailment of the S–O distance. In A-TS_1 species, it can be readily seen that oxygen atom is closer to iron atom ($r_{Fe\text{-}O}$=1.734 Å LS and 1.832 Å HS) than to sulfur atom (r_{S-O} = 2.278 Å LS and 2.044 Å HS). Therefore, A-TS_1 species is more reactant like in character. Particularly, this reactant-like character of A-$^2TS_1$ on LS state is more obvious than A-$^4TS_1$ on HS state. In the product complex A-PC species, A-^{2}PC and A-^{4}PC, a double bond is formed between oxygen and S_5 atoms (r_{S-O} = 1.728 Å LS and 1.700 Å HS). Concomitantly, the Fe–O bond is elongated to be 2.029 Å LS and 2.370 Å HS.

The spin density distribution for the stationary points involved in S_5-oxidation is listed in Table S1. In the A-RC species, spin density is localized on Cpd I. Then, it shifts from the oxygen, –SH ligand and porphyrin to the iron and sulfur atom of chlorpromazine. In A-TS_1 species, the accumulation of spin density on sulfur atom indicates the partial formation of S–O and Fe–O single bonds, resulting in the occurrence of an unpaired electron on sulfur atom. As the reaction proceeds, the unpaired electron on sulfur further pairs with the electron of oxygen atom residing on Fe–O single bond to produce the S=O double bond in A-PC species. Simultaneously, Fe–O single bond is cleaved. There is no spin density on sulfur atom any more. Spin density is mainly localized on iron on both LS and HS states. All the results clearly indicate a stepwise transfer of two electrons.

The calculated energy profiles for S_5-oxidation (path A) are shown in Fig. 2. The LS/HS energy barrier of path A is 9.6/14.1 kcal/mol in the gas phase, which corresponds to 8.7/12.9 kcal/mol when ZPE correction and the bulk polarity effect are incorporated. The oxidation process is endothermic with the reaction energy of 21.6 kcal/mol LS and 7.9 kcal/mol HS in chlorobenzene. The lower LS energy barrier agrees well with the more reactant-like character of A-$^2TS_1$ than of A-$^4TS_1$ as discussed above. It can be readily seen that the solvation of chlorobenzene contributes to the barrier decrease in path A. The energy gap between A-$^2TS_1$ and A-$^4TS_1$ is large to be 4.2 kcal/mol in chlorobenzene. The ratio of the reaction rate on the LS/HS route is 1198:1. As a consequence, S_5-oxidation of chlorpromazine by Cpd I proceeds mainly in a SSM mechanism. The LS state of Cpd I is more feasible than the HS state.

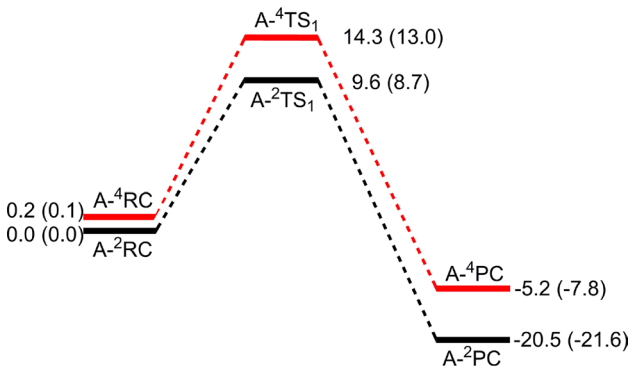

Fig. 2 Energy profiles (in kcal/mol) for S_5-oxidation (path A) of chlorpromazine by Cpd I (values out of parentheses, relative energies in the gas phase; values in parentheses, relative energies in chlorobenzene. Definitions are the same in the following energy profile figures)

3.2 Aromatic hydroxylation (paths B and C)

Owning to the similar properties of C_7 and C_8 sites, the hydroxylations of chlorpromazine at C_7 (path B) and C_8 (path C) sites have been explored for comparison. Aromatic hydroxylation process begins with the nucleophilic addition of Cpd I's oxygen atom at the carbon atom to form the oxidized chlorpromazine intermediate, which then converts into the hydroxylated chlorpromazine metabolite via intramolecular 1,2-proton transfer (Scheme 2b).

3.2.1 Nucleophilic addition of Cpd I's oxygen atom

The optimized geometries of all the stationary points for the initial nucleophilic addition of Cpd I's oxygen atom along paths B and C are shown in Fig. 3. For C_7-hydroxylation (path B), the located transition-state B-TS_1 species, B-$^2TS_1$ and B-$^4TS_1$, is characterized by its single imaginary frequency of 269.0i cm^{-1} LS and 440.1i cm^{-1} HS (Fig. 3a). Animation of the single imaginary frequency of B-TS_1 species indicates the migration of heavy oxygen atom from Fe atom to C_7 atom, leading to the C_7–O bond formation. Compared with reactant complex B-RC species, B-^{2}RC and B-^{4}RC, the Fe–O bond in the transition-state B-TS_1 species is elongated by 0.077 Å LS and 0.094 Å HS, which is concurrent with the curtailment of the C_7–O distance by 1.382 Å LS and 1.438 Å HS. In B-TS_1 species, the distance of Fe–O bond is elongated to be 1.727 Å LS and 1.747 Å HS, while the C_7–O distance is shorten to be 1.948 Å LS and 1.851 Å HS. It can be readily seen that oxygen atom is closer to iron atom than to C_7 atom. So B-TS_1 species is still more reactant-like in character. Particularly, the reactant-like characters of B-$^2TS_1$ are more obvious than HS transition-state B-$^4TS_1$. In the intermediate B-IM species, B-^{2}IM and B-^{4}IM, a single bond is formed between oxygen and C_7 atom with the C_7–O bond length of 1.469 Å LS and 1.488 Å HS. Simultaneously, the Fe–O bond is further elongated to be 1.920 Å LS and 1.823 Å HS.

Considering C_8-hydroxylation (path C), as shown in Fig. 3b, the transition-state C-TS_1 species, C-$^2TS_1$ and C-$^4TS_1$, located for the nucleophilic attack of Cpd I's oxygen atom is characterized by its single imaginary frequency of 314.6i cm^{-1} LS and 465.5i cm^{-1} HS. Animation of the single imaginary frequency of C-TS_1 species also concerns the motion of heavy oxygen atom from Fe atom to C_8 atom, leading to the C_8–O bond formation.

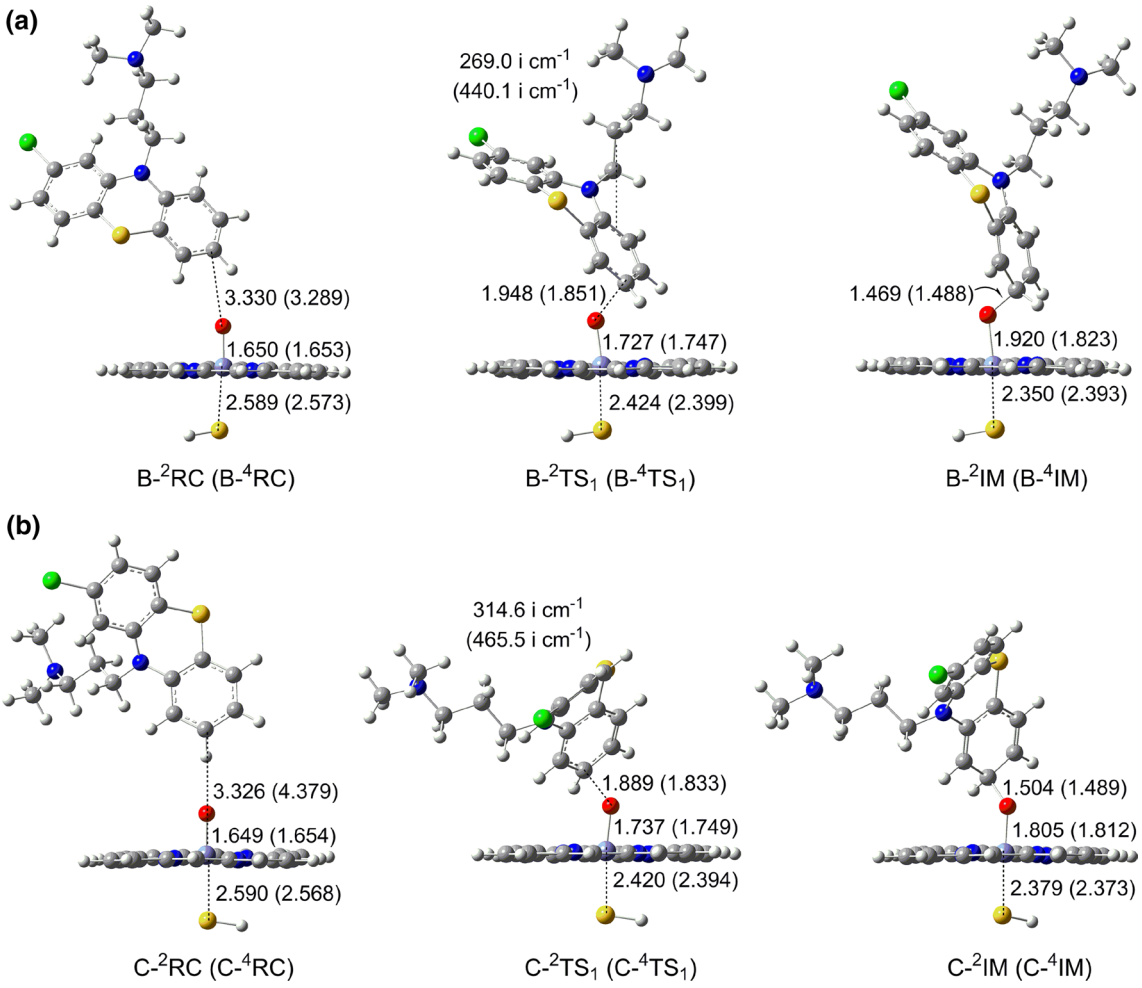

Fig. 3 Optimized structures (in Å) for the nucleophilic attack of Cpd I's oxygen atom at C_7 (**a**, path B) and C_8 (**b**, path C) sites of chlorpromazine at the B1 level

The geometrical feature tendencies for the nucleophilic addition of Cpd I's oxygen atom along path C are similar to path B on either the LS or the HS state: The Fe–O distance in C-TS$_1$ species is elongated by 0.088 Å LS and 0.095 Å HS with respect to its corresponding reactant complex C-RC species, C-^{2}RC and C-^{4}RC, and the C_8–O distance is dramatically shorted by 1.437 Å LS and 2.546 Å HS. In C-TS$_1$ species, the distance of Fe–O bond is 1.737 Å LS and 1.749 Å HS and the C_8–O distance is 1.889 Å LS and 1.833 Å HS, indicating the partial formation of C_8–O bond. It can be readily seen that oxygen atom is also closer to iron atom than to C_8 atom. Thus, C-TS$_1$ species is still more reactant-like in character and the reactant-like character of C-^{2}TS$_1$ is more obvious than C-^{4}TS$_1$. In the intermediate C-IM species, C-^{2}IM and C-^{4}IM, a single bond is formed between oxygen and C_8 atom. The C_8–O bond length is 1.504 Å LS and 1.489 Å HS, and the Fe–O bond is elongated to be 1.805 Å LS and 1.812 Å HS.

The spin density distribution of the stationary points involved in the nucleophilic addition processes of paths B and C is listed in Table S2. In the reactant complexes, spin density mainly delocalizes on Cpd I. As the nucleophilic addition proceeds, spin density migrates from the oxygen, –SH ligand and porphyrin to the iron atom and chlorpromazine. In B-TS$_1$ and C-TS$_1$ species, high spin density resides on iron and chlorpromazine. The accumulation of spin density on the beta carbon atom (C_8 atom in path B and C_7 atom in path C) implies the emergence of an unpaired electron. Further delocalization appears in the B-^{4}IM and C-^{4}IM, with a significant amount of the spin density on chlorpromazine delocalized in the direction of beta carbon. After the nucleophilic addition, spin density is localized on Cpd I on LS state and delocalized between Cpd I and chlorpromazine on HS state.

The calculated energy profiles for the nucleophilic addition of Cpd I's oxygen atom along paths B and C are shown in Fig. 4. As shown in Fig. 4, the gas-phase

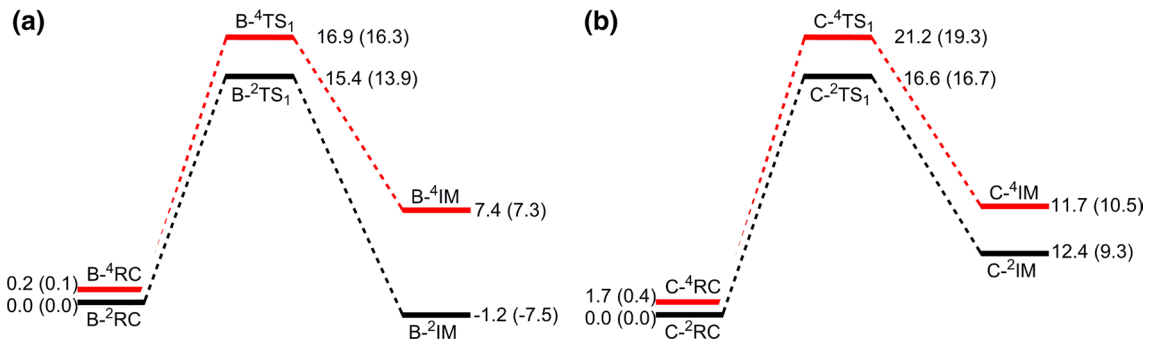

Fig. 4 Energy profiles (in kcal/mol) for the nucleophilic attack of Cpd I's oxygen atom at C_7 (**a**, path B) and C_8 (**b**, path C) sites of chlorpromazine

LS/HS energy barrier is 15.4/16.7 kcal/mol for B-TS_1 species and 16.6/19.5 kcal/mol for C-TS_1 species, which correspond to 13.9/16.2 and 16.7/18.9 kcal/mol when ZPE correction and the bulk polarity effect are incorporated. The energy gap between LS and HS is 2.3 kcal/mol for B-TS_1 species and 2.2 kcal/mol for C-TS_1 species in chlorobenzene. The lower LS energy barriers of B-$^2TS_1$ and C-$^2TS_1$ with respect to B-$^4TS_1$ and C-$^4TS_1$ arise from their more reactant-like characters. The ratio of the reaction rate on the LS/HS route is 48.5:1 for B-TS_1 species and 34.6:1 for C-TS_1 species. Consequently, the nucleophilic addition processes along paths B and C proceed predominantly via the LS state in the SSM mechanism.

3.2.2 *Intramolecular proton transfer*

In this step, the formed intermediate B-IM species (B-^{2}IM and B-^{4}IM) and C-IM species (C-^{2}IM and C-^{4}IM) can convert to its enol form product complexes B-PC species (B-^{2}PC and B-^{4}PC) and C-PC species (C-^{2}PC and C-^{4}PC) via intramolecular proton transfer. Owning to the strong interaction between Fe and oxygen atoms in B-IM and C-IM species (r_{Fe-O} = 1.805–1.920 Å), this proton transfer should be an enzymatic process. Considering the presence of one explicit water molecule in the active site of the human P450 1A2 [25], both the direct and one-water-assisted enzymatic proton transfer mechanisms were taken into account for comparison. The optimized structures of transition states and calculated energy profiles for the intramolecular proton transfer processes of paths B and C are shown in Figs. 5 and 6, respectively.

For the direct reaction mechanism, the located transition state B-TS_2 species (B-$^2TS_2$ and B-$^4TS_2$) and C-TS_2 species (C-$^2TS_2$ and C-$^4TS_2$) are all triangle structures. The single imaginary frequencies of B-TS_2 and C-TS_2 species are greater than 1200i cm^{-1}, which mainly comprises the motion of the light hydrogen atom from the alpha carbon (C_7 atom in path B and C_8 atom in path C) to the bonding oxygen atom. The gas-phase LS/HS energy barrier is 12.5/17.1 kcal/mol for B-TS_2 species and 9.8/11.4 kcal/mol for C-TS_2 species, which corresponds to 16.0/12.7 and 12.3/8.9 kcal/mol when ZPE correction and the bulk polarity effect are incorporated. Both proton transfer processes are exothermic with the reaction energies of 47–60 kcal/mol in chlorobenzene.

With the presence of one explicit water molecule, a water bridge is formed, receiving a proton and donating one in turn. The B-TS_{2w} and C-TS_{2w} species involved, B-$^{2,4}TS_{2w}$ and C-$^{2,4}TS_{2w}$, is expanded to be pentagon structure, which is characterized by the single imaginary frequency of 49–184 i cm^{-1}. Animation of the single imaginary frequency of B-TS_{2w} and C-TS_{2w} species shows the synchronous transfers of two hydrogen atoms, namely H atom from alpha C atom to O_w atom of the water molecule and the H_w atom of water molecule from O_w to O atoms. The gas-phase LS/HS activation energy is 2.7/7.6 kcal/mol for B-TS_{2w} species and −0.7/0.4 kcal/mol for C-TS_{2w} species, which corresponds to 4.8/6.8 and −0.4/0.6 kcal/mol when ZPE correction and the bulk polarity effect are incorporated. The water-assisted proton transfer processes are still exothermic with the reaction energies of 43–55 kcal/mol in chlorobenzene. As expected, the water-assisted energy barriers are dramatically lower than those of the direct reaction processes by 6–12 kcal/mol, attributed to the lower constraint of the pentagon transition state structures, where the energies required for the bond dissociation and formation are smaller than the triangle so much that a large amount of deformation energy is saved. It suggests that the presence of the explicit water is thermodynamically and kinetically beneficial to this proton transfer process. Additionally, the reactant complexes on LS state, B-^{2}IM and C-^{2}IM, are much more stable than those on HS state, B-^{4}IM and C-^{4}IM, indicating clearly that this proton transfer process still proceeds in a SSM mechanism, mainly via the LS state of Cpd I.

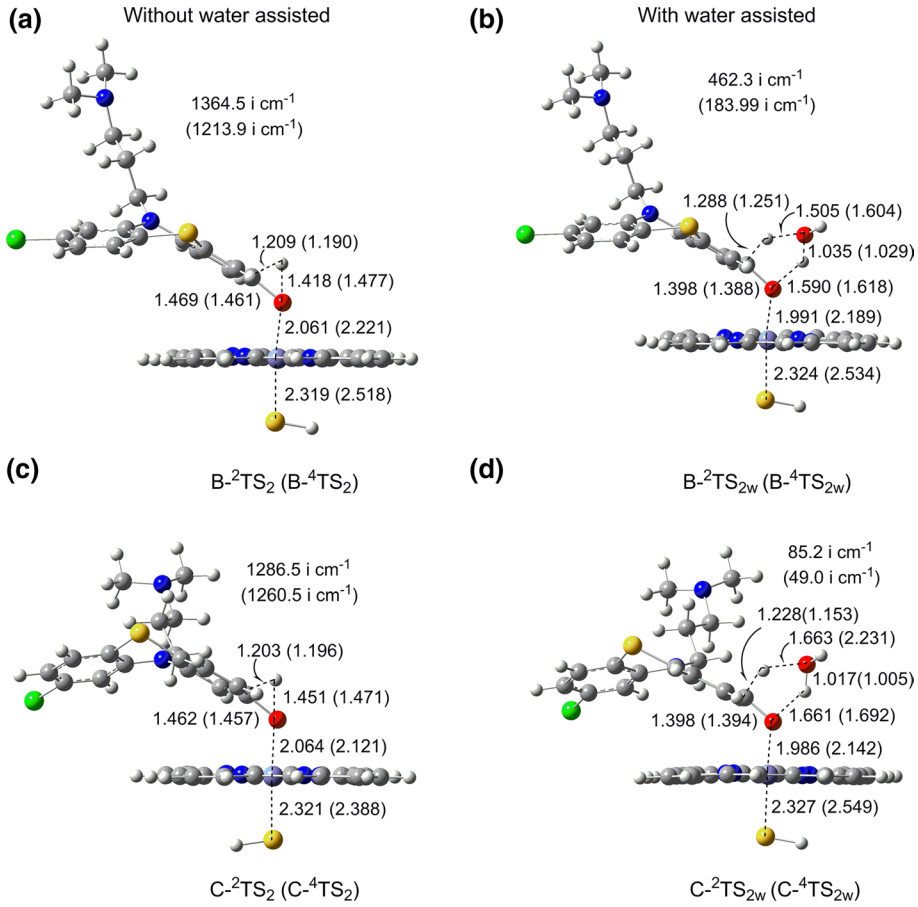

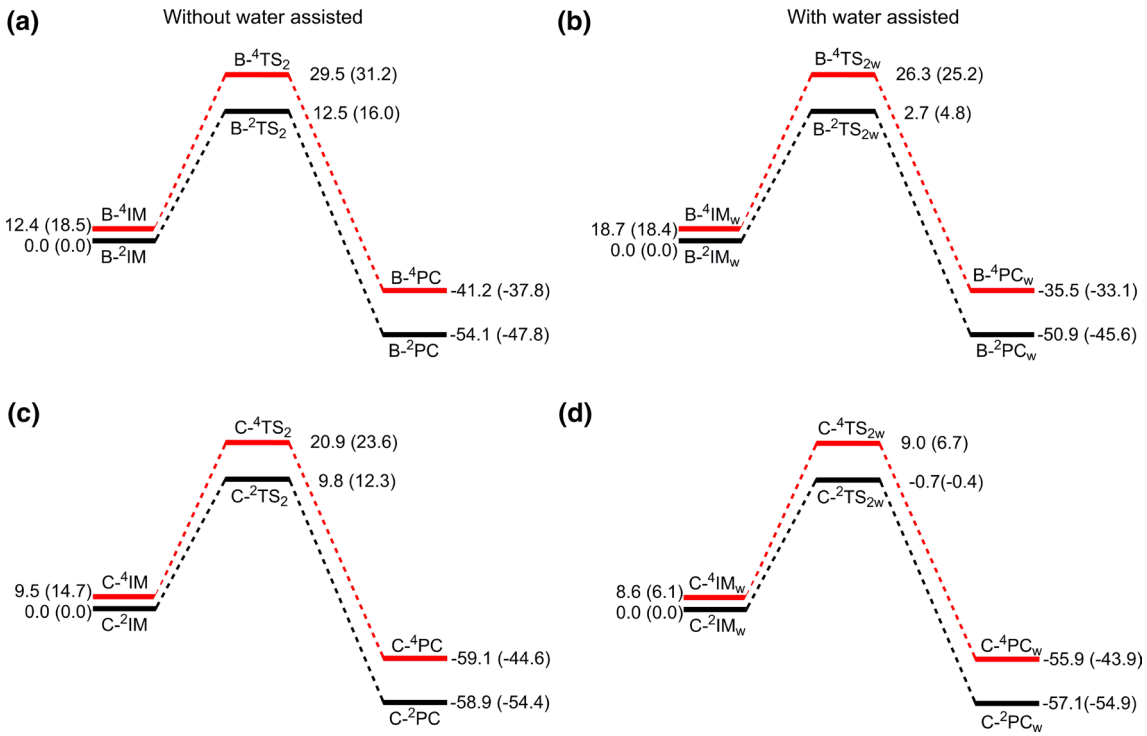

Fig. 5 Optimized transition state structures (in Å) for the intramolecular proton transfer along paths B (**a**, **b**) and C (**c**, **d**) at the B1 level

Fig. 6 Energy profiles (in kcal/mol) for the intramolecular proton transfer for the intramolecular proton transfer along paths B (**a**, **b**) and C (**c**, **d**)

As a result, the rate-determining steps along the potential energy surfaces of paths B and C both involve the nucleophilic attack of Cpd I's oxygen atom, each of which proceeds predominantly via the LS state in the SSM mechanism. Path B is thermodynamically and kinetically more favorable than path C due to its lower activation barrier, and 7-hydroxychlorpromazine therefore is the optimum aromatic hydroxylation product of chlorpromazine by Cpd I.

3.3 *N*-demethylation (paths D1 and D2)

As depicted in Scheme 2c, the overall reaction of CYP-catalyzed *N*-dealkylation of chlorpromazine proceeds through two stepwise stages, *N*-methyl hydroxylation and C–N bond fission to release formaldehyde.

3.3.1 N-methyl hydroxylation

For *N*-methyl hydroxylation, the reaction pattern starts with proton abstraction from methyl group to the Cpd I's oxygen atom, forming a *N*-methylene intermediate, which then acts as a receptor of hydroxyl from the active iron species by oxygen-rebound process. The reaction is concerted on the LS state, forming carbinolamine–heme complex without a distinct oxygen-rebound step. The high-spin proton transfer intermediate, ^{4}INT, just serves as a shoulder but not a real minimum and fall to the corresponding carbinolamine–heme complex with a barrier-free oxygen rebound. Therefore, the *N*-methyl hydroxylation is an effective concerted process on the two spin states. These results are in agreement with our recent work [30] and follow earlier observation on P450 reactions [35, 44].

The optimized geometries of all the stationary points for the *N*-methyl hydroxylations of paths D1 and D2 are shown in Fig. 7. As for path D1, the mono-*N*-demethylation, the transition state D1-TS$_1$ species, D1-^{2}TS$_1$ and D1-^{4}TS$_1$, located for *N*-methyl hydroxylation is characterized by its single imaginary frequency of 604.1i cm^{-1} LS and 1032.0i cm^{-1} HS. Animation of the single imaginary frequency of D1-TS$_1$ species comprises the motion of hydrogen from methyl carbon atom to the oxygen atom of Cpd I atom. Compared with the reactant complex D1-RC species, D1-^{2}RC and D1-^{4}RC, it can be seen that the Fe–O bond is elongated by 0.049 Å LS and 0.082 Å HS in the transition state D1-TS$_1$ species, whereas the O–H distance is considerably reduced by 0.817 Å LS and 0.856 HS. This is accompanied by the elongation of the C–H bond by 0.082 Å LS and 0.174 Å HS. Transition-state D1-TS$_1$ species is characterized by an almost collinear arrangement of the C–H–O atoms with the bond angles of 170.9° LS and 171.3° HS. The geometric parameters in Fig. 7 also indicate the degrees of C–H bond cleavage in the D1-TS$_1$ species. In the D1-TS$_1$ species, hydrogen atom is closer to

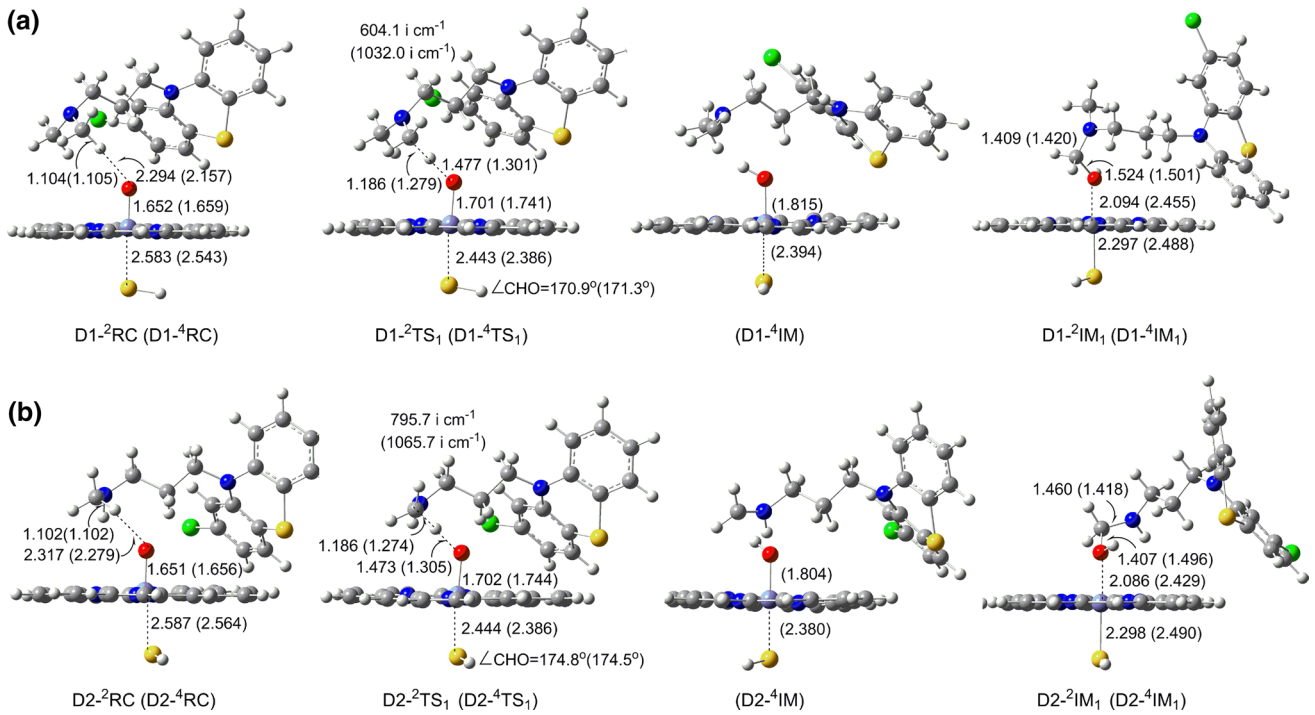

Fig. 7 Optimized structures (in Å) for the *N*-methyl hydroxylation in mono-*N*-demethylation (**a**, path D1) and di-*N*-demethylation (**b**, path D2) of chlorpromazine by Cpd I at the B1 level

carbon atom (r_{C-H} = 1.186 Å LS and 1.279 Å HS) than to oxygen atom (r_{O-H} = 1.477 Å LS and 1.301 Å HS). Therefore, they are more reactant like in character. Furthermore, the reactant-like character of D1-^{2}TS$_1$ on the LS state is more obvious than of D1-^{4}TS$_1$ on the HS state. As the reaction progresses from D1-RC species to the intermediate D1-IM$_1$ species, D1-^{2}IM$_1$ and D1-^{4}IM$_1$, the distances between the SH ligand and Fe are shortened by 0.286 Å LS and 0.055 Å HS.

As for the di-*N*-demethylation path D2, the located transition-state D2-TS$_1$ species, D2-^{2}TS$_1$ and D2-^{4}TS$_1$, is characterized by its single imaginary frequency of 795.7 i cm^{-1} LS and 1065.7 i cm^{-1} HS. Animation of the single imaginary frequency of C-TS$_1$ species also concerns the motion of hydrogen from methyl carbon atom to the oxygen atom of Cpd I atom. The geometrical feature tendencies for the *N*-methyl hydroxylation along path D2 are similar to path D1. The Fe–O bonds in the transition-state D2-TS$_1$ species are elongated by 0.051–0.088 Å, while the O–H distances are reduced by 0.817–0.856 Å. This is accompanied by the elongation of the C–H bonds by 0.084–0.172 Å. Transition-state D2-TS$_1$ species also exhibits an almost collinear arrangement of the C–H–O atoms with the bond angles of 174.5–174.8° and the reactant-like character. In the D2-TS$_1$ species, hydrogen atom is closer to carbon atom (r_{C-H} = 1.186 Å LS and 1.274 Å HS) than to oxygen atom (r_{O-H} = 1.473 Å LS and 1.305 Å HS). Clearly, the reactant-like character of D1-^{2}TS$_1$ on the LS state is still more obvious than of D1-^{4}TS$_1$ on the HS state. In the intermediate D2-IM$_1$ species, D2-^{2}IM$_1$ and D2-^{4}IM$_1$, the distances between the SH ligand and Fe are shortened by 0.074–0.289 Å.

The spin density distribution for the stationary points involved in the *N*-methyl hydroxylations of paths D1 and D2 is reported in Table S3. Initially, spin density is localized on Cpd I. Then, during the C–H bond activation step it shifts from the oxygen, –SH ligand and porphyrin to the Fe and chlorpromazine. When reaching D1-TS$_1$ species and D2-TS$_1$ species, high spin density resides on the nitrogen atom of chlorpromazine and the iron. The accumulation of spin density on nitrogen in D1-^{2}TS$_1$ and D2-^{2}TS$_1$ suggests that it may be involved in the stabilization of carbon during leaving of the hydrogen atom. In D1-^{4}TS$_1$ and D2-^{4}TS$_1$, there is some spin density locating on the carbon of chlorpromazine. On the porphyrin, on the other hand, excess unpaired spin is no longer observed and spin density is delocalized between Fe-oxo and –SH. Further delocalization appears in the D1-^{4}IM and D2-^{4}IM, with a significant amount of the spin density on chlorpromazine delocalized in the direction of carbon. There is also accumulation of the spin density on iron by a shift from –SH and oxygen. After the hydroxyl rebound step, spin density is localized on iron on the LS and delocalized between iron and –SH on the HS. All the observations indicate that the *N*-methyl hydroxylations of paths D1 and D2 proceed via the SET mechanism.

The calculated energy profiles for the *N*-methyl hydroxylations of paths D1 and D2 are shown in Fig. 8. The gas-phase LS/HS energy barrier is 4.7/3.3 kcal/mol for D1-TS$_1$ species and 6.4/5.1 kcal/mol for D2-TS$_1$ species, which decrease to 1.9/1.9 and 4.5/4.3 kcal/mol when ZPE correction and the bulk polarity effect are incorporated. The energy gaps between LS and HS of D1-^{2}TS$_1$ and D2-^{2}TS$_1$ species are approximately zero in chlorobenzene, indicating a TSR mechanism. The *N*-methyl hydroxylation is greatly exothermic with the reaction energies of 44–61 kcal/mol in chlorobenzene.

3.3.2 *C–N bond fission*

As the second step of the *N*-demethylation, C–N bond fission requires a proton transfer from the hydroxyl oxygen to nitrogen atom, while the C–N bond between the alpha carbon and nitrogen gradually breaks. We examined two

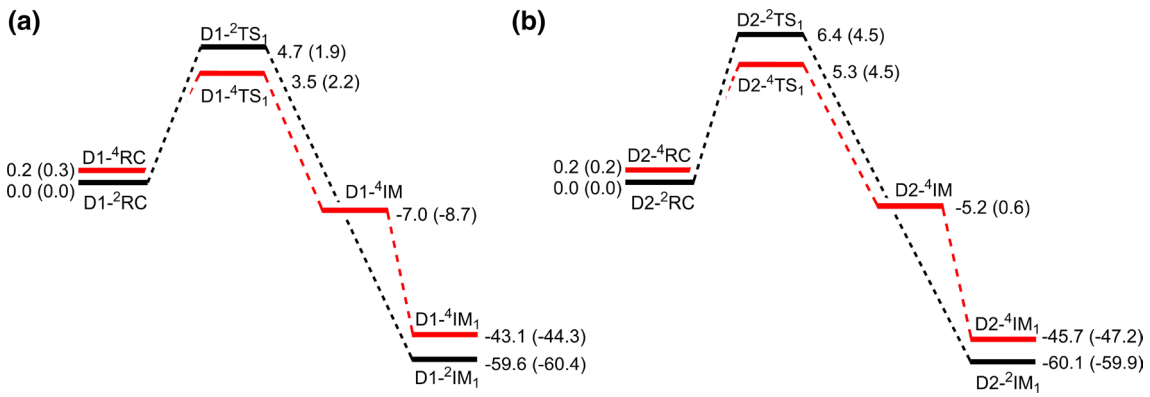

Fig. 8 Energy profiles (in kcal/mol) for the *N*-methyl hydroxylation in mono-*N*-demethylation (**a**, path D1) and di-*N*-demethylation (**b**, path D2) of chlorpromazine by Cpd I

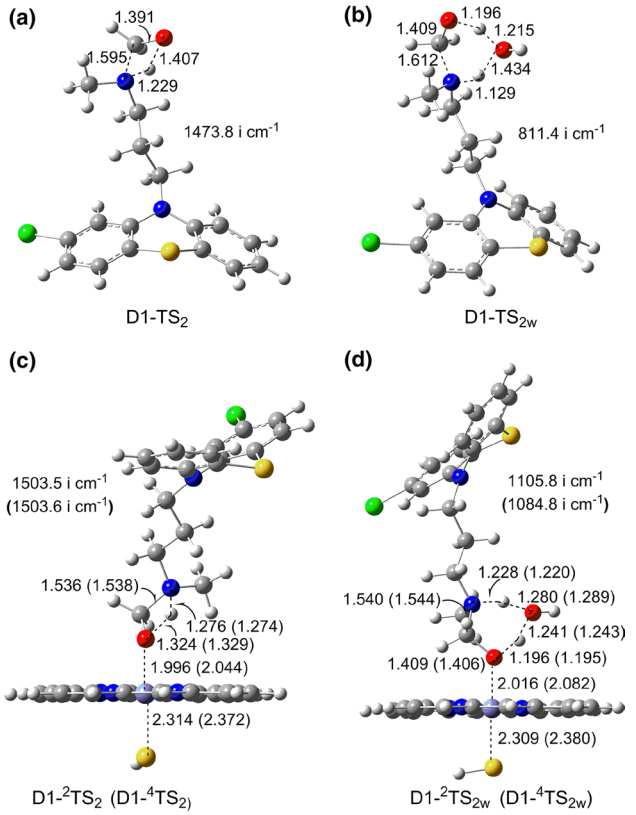

Fig. 9 Optimized transition-state structures (in Å) for the C–N fission along the mono-*N*-demethylation (path D1) of chlorpromazine by Cpd I at the B1 level

different processes for the second step: the direct proton transfer and the water-assisted proton transfer. Both the enzymatic and nonenzymatic environments were taken into account.

The optimized transition state structures and energy profiles for the C–N bond fission along path D1 are depicted in Figs. 9 and 10, respectively. For the direct proton transfer process, the enzymatic and nonenzymatic transition states (D1-$^{2,4}TS_2$ and D1-TS_2) are all rhomboid structures, whose single imaginary frequencies are greater than 1473i cm^{-1}. Animation of the single imaginary frequency shows the direct motion of hydroxyl hydrogen to nitrogen atom. For the water-assisted proton transfer process, the involved enzymatic and nonenzymatic transition states (D1-$^{2,4}TS_{2w}$ and D1-TS_{2w}) are expanded to be hexagon structures. Their single imaginary frequencies range from 811 to 1105i cm^{-1}, wherein the water molecule hydrogen bonding with the nitrogen gradually transfers a proton to the nitrogen, while the hydroxyl proton gradually transfers to the water oxygen. Figure 10 shows that the gas-phase energy barriers of the direct proton transfer are 36.1 and 27.8/21.1 kcal/mol for the nonenzymatic and enzymatic LS/HS environments, respectively, which decrease to 30.3 and 23.5/20.1 kcal/mol when ZPE correction and the bulk polarity effect are incorporated. For the water-assisted proton transfer process, the nonenzymatic and enzymatic LS/HS energy barriers are 17.0 and 11.4/11.8 kcal/mol, respectively, in the gas-phase, which decrease to 13.8 and 9.5/10.1 kcal/mol when ZPE correction and the bulk polarity effect are incorporated. Clearly, with the assistance of one explicit water molecule, the energy barrier required for C–N fission is dramatically lowered by 10–17 kcal/mol in chlorobenzene. The large barrier decrease in the water-assisted proton transfer process can be derived from the smaller ring tension of the hexagon compared with rhomboid. Furthermore, the water-assisted enzymatic LS/HS energy barrier is 4.3/3.7 kcal/mol lower than the nonenzymatic energy barrier in chlorobenzene. The binding energy of the carbinolamine to heme in path D1 is 4.2 kcal/mol LS and 1.0 kcal/mol HS (Table S4). The lower binding energy on HS state results in the higher energy of the carbinolamine on HS state (15.5 kcal/mol higher than that on LS state in chlorobenzene). Comparison of the above barrier data with the binding energies of carbinolamine to heme shows that C–N fission proceeds in an enzymatic route, predominately via the LS state.

Figures 11 and 12 show the optimized transition state structures and energy profiles for the C–N bond fission along path D2, respectively. Analog to path D1, the enzymatic and nonenzymatic transition states (D2-$^{2,4}TS_2$ and D2-TS_2) involved in the direct proton transfer process of path D2 are also rhomboid structures, which expand to be the hexagon structures of D2-$^{2,4}TS_{2w}$ and D2-TS_{2w} in the water-assisted proton transfer process. For the direct proton transfer process, the gas-phase nonenzymatic and enzymatic LS/HS energy barriers are 37.6 and 28.0/30.8 kcal/mol, respectively, which decrease to 31.4 and 24.3/27.7 kcal/mol when ZPE correction and the bulk polarity effect are incorporated. With the assistance of one explicit water molecule, the gas-phase nonenzymatic and enzymatic LS/HS energy barriers are 18.5 and 11.6/12.4 kcal/mol, respectively, which decrease to 14.7 and 9.7/10.6 kcal/mol when ZPE correction and the bulk polarity effect are incorporated. By comparison, it can be readily seen that the energy barriers involved in the water-assisted proton transfer processes are 14–17 kcal/mol lower than those of the direct proton transfer in chlorobenzene. Comparison of the above barrier data with the binding energies of carbinolamine to heme (LS: 5.0 kcal/mol; HS: 1.5 kcal/mol, Table S4) indicates that C–N fission should happen in a water-assisted enzymatic environment, mainly via the LS state.

Taken together, the C–N bond fission proceeds mainly via the water-assisted enzymatic proton transfer process on LS state. *N*-methyl hydroxylation is the rate-determining step along the potential energy surface of either mono-*N*-demethylation (path D1) or di-*N*-demethylation (path D2).

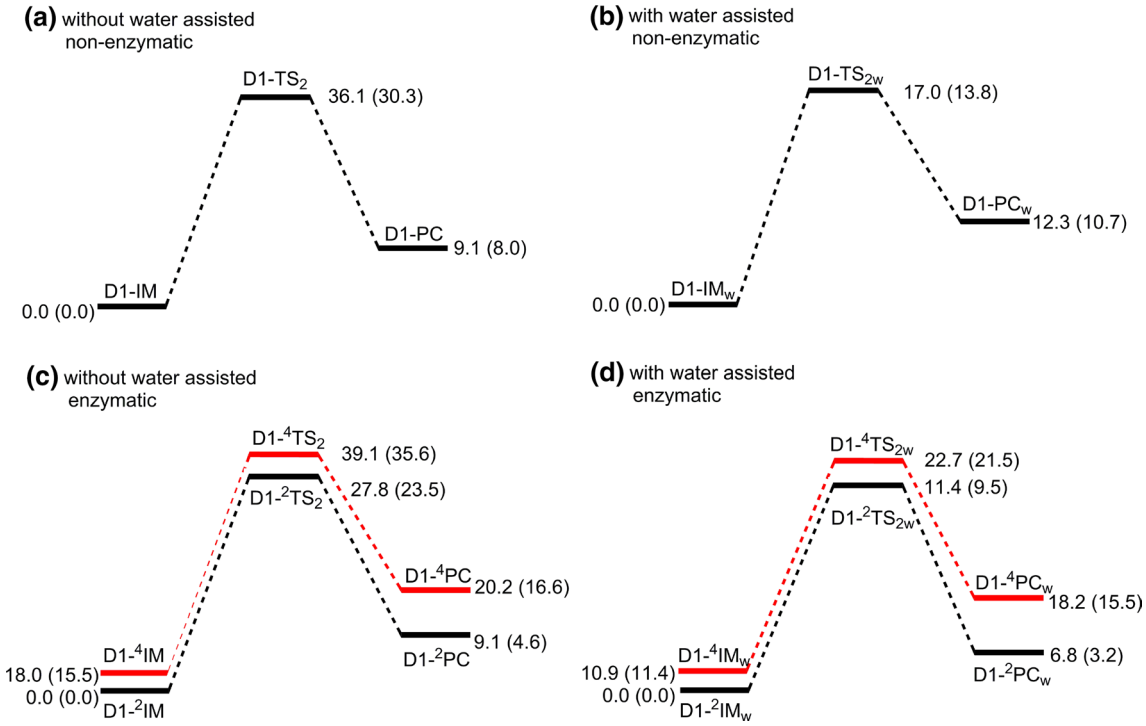

Fig. 10 Energy profiles (in kcal/mol) for the C–N fission along the mono-*N*-demethylation (path D1) of chlorpromazine by Cpd I at the B1 level

In summary, the LS/HS activation barriers for the rate-determining steps of S_5-oxidation (path A), aromatic hydroxylations at C_7 (C_7-hydroxylation, path B) and C_8 (C_8-hydroxylation, path C) sites as well as mono-*N*-demethylation (path D1) and di-*N*-demethylation (path D2) are 8.7/12.9, 13.9/16.2, 16.7/18.9, 1.9/1.9 and 4.5/4.3 kcal/mol, respectively, in chlorobenzene. It can be concluded that *N*-demethylation, paths D1 and/or D2, is the most plausible metabolic pathway of chlorpromazine catalyzed by CYP1A2 on either LS or HS state, followed by paths A, B and C in turn. So mono-*N*-desmethylchlorpromazine (D1-PC) is the optimum metabolite of chlorpromazine, which can undergo the second *N*-demethylation to yield di-*N*-desmethylchlorpromazine (D2-PC). All the observations agree well with the experimental results [12]. Generally, all the metabolic pathways proceed in a SSM mechanism, mainly through the LS state.

4 Conclusions

The metabolic mechanisms of chlorpromazine catalyzed by CYP1A2 have been systematically addressed in the present work based on DFT calculation. The mechanistic conclusions have been revealed as follows. S_5-oxidation (path A) is a one-step reaction, which involves a stepwise transfer of two electrons. The rate-determining step of aromatic

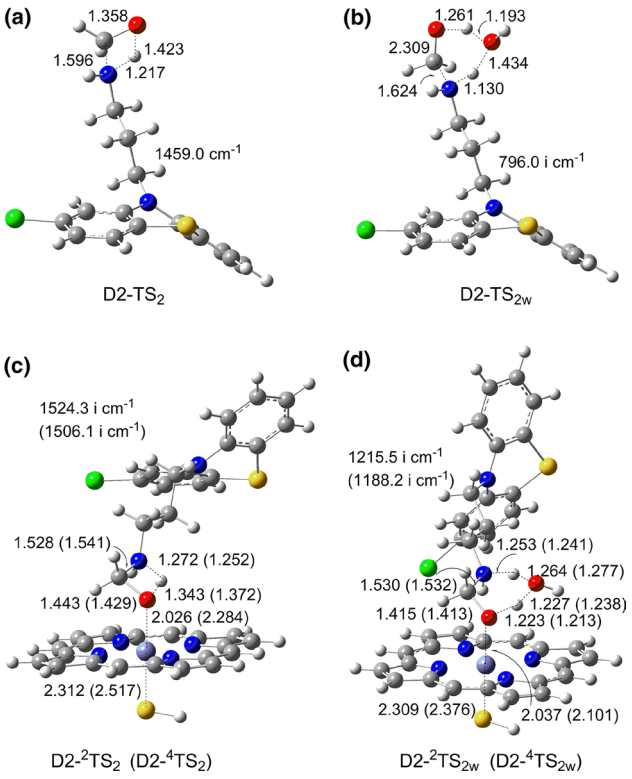

Fig. 11 Optimized transition state structures (in Å) for the C–N fission along the di-*N*-demethylation (path D2) of chlorpromazine by Cpd I at the B1 level

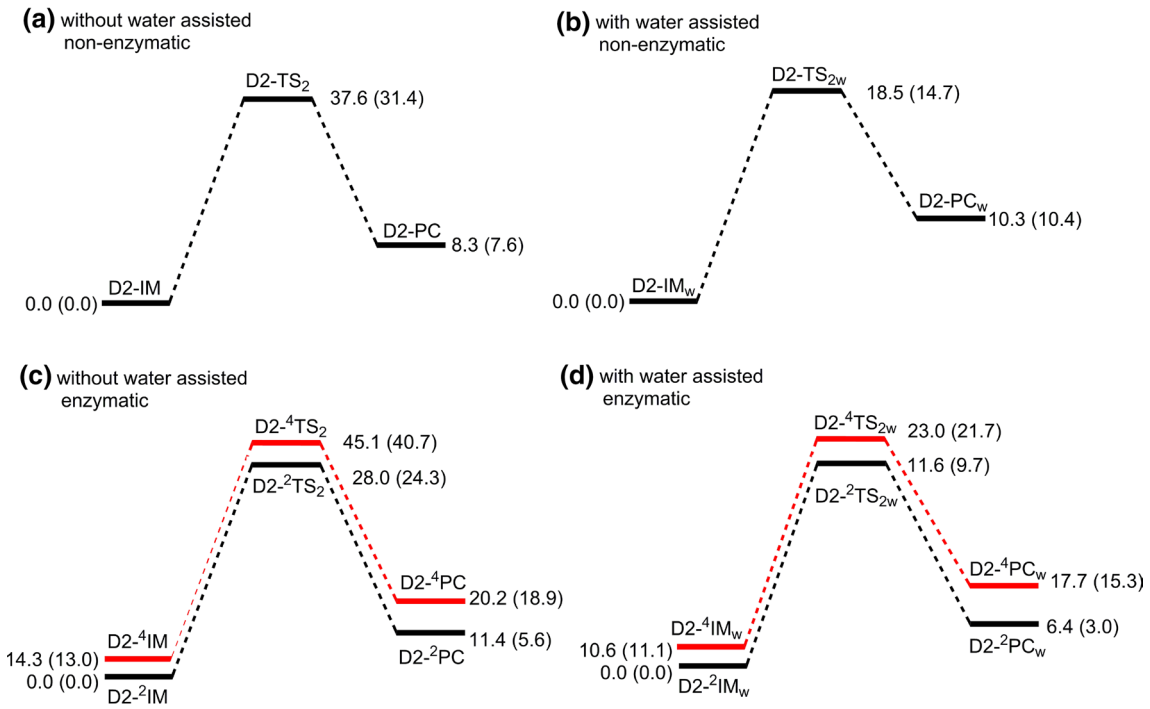

Fig. 12 Energy profiles (in kcal/mol) for the C–N fission along the di-*N*-demethylation (path D2) of chlorpromazine by Cpd I at the B1 level

hydroxylation (paths B and C) involves the nucleophilic addition of Cpd I's oxygen atom. The subsequent intramolecular proton transfer is prone to the water-assisted enzymatic proton transfer mechanism. *N*-methyl hydroxylation is the rate-limiting step of *N*-demethylation, which proceeds predominantly via a SET mechanism. The generated carbinolamines then prefer to decomposition in a water-assisted enzymatic process on LS state. *N*-demethylation is the most thermodynamically and kinetically feasible metabolic pathway of chlorpromazine due to its lowest activation barrier, followed by path A. Mono-*N*-desmethylchlorpromazine therefore is the most feasible chlorpromazine metabolite catalyzed by CYP1A2, followed by di-*N*-desmethylchlorpromazine, chlorpromazine 5-sulfoxide, 7-hydroxychlorpromazine and 8-hydroxychlorpromazine. Each metabolic pathway proceeds in a SSM mechanism, predominately via the LS state of Cpd I. Our results keep in good accordance with the experimental observations, which can provide some complementary insights into the *N*-dealkylation mechanism by CYP and offer general implications for the metabolic mechanism of chlorpromazine-like drugs.

5 Supporting information

Spin densities for the species involved in the metabolic processes of chlorpromazine, binding energies of carbinolamine to heme in the *N*-demethylation of chlorpromazine and cartesian coordinates of all stationary points along the potential energy profiles.

Acknowledgments This work was supported by grants from National Natural Science Foundation of China (Grant No. 21203153), Science and Technology Department of Sichuan Province (Grant No. 2011JY0136) and Department of Education of Sichuan Province (Grant No. 12ZA174) and China West Normal University (Grant No. 11B002).

References

1. Liu X, De Haan S (2009) Cochrane Database Syst Rev 2:CD007778
2. Anthérieu S, Bachour-El Azzi P, Dumont J, Abdel-Razzak Z, Guguen-Guillouzo C, Fromenty B, Robin MA, Guillouzo A (2013) Hepatology 57:1518–1529
3. Tohen M, Vieta E (2009) Bipolar Disord 2:45–54
4. Morak-Młodawska B, Jeleń M (2007) Pol Merkur Lek 23:459–461
5. Shin SY, Kim CG, Kim SH, Kim YS, Lim Y, Lee YH (2010) Exp Mol Med 42:395–405
6. Liperoti R, Pedone C, Corsonello A (2008) Curr Neuropharmacol 6:117–124
7. Drucker AM, Rosen CF (2011) Drug Saf 34:821–837
8. Lasic D, Cvitanovic MZ, Uglešic B, Višic V, Hlevnjak I (2011) Psychiatr Danub 23:194–197
9. Shahzad S, Suleman MI, Shahab H, Mazour I, Kaur A, Rudzinskiy P, Lippmann S (2002) Psychosomatics 43:354–359
10. Subashini K, Rao VA (2004) Indian J Pharmacol 36:323–324
11. Toler SM (2004) Exp Biol Med (Maywood) 229:607–615
12. Wójcikowski J, Boksa J, Daniel WA (2010) Biochem Pharmacol 80:1252–1259

13. Daniel W (1995) Pol J Pharmacol 47:367–379
14. Chetty M, Pillay VL, Moodley SV, Miller R (1996) Eur Neuropsychopharmacol 2:85–91
15. Chetty M, Gouws E, Miller R, Moodley SV (1999) Eur Neuropsychopharmacol 9(1–2):77–82
16. Abernathy CO, Lukacs L, Zimmerman HJ (1977) Proc Soc Exp Biol Med 155:474–478
17. Tavoloni N, Boyer JL (1980) J Pharmacol Exp Ther 214:269–274
18. Wójcikowski J, Pichard-Garcia L, Maurel P, Daniel WA (2003) Br J Pharmacol 138:1465–1474
19. Wójcikowski J, Pichard-Garcia L, Maurel P, Daniel WA (2004) Eur Neuropsychopharmacol 14:199–208
20. Wójcikowski J, Maurel P, Daniel WA (2006) Drug Metab Dispos 34:471–476
21. Chetty M, Miller R, Moodley SV (1994) Eur J Clin Pharmacol 46:523–526
22. Kot M, Daniel WA (2008) Biochem Pharmacol 76:543–551
23. Blomberg MRA, Borowski T, Himo F, Liao RZ, Siegbahn PEM (2014) Chem Rev 114:3601–3658
24. Schrŏder D, Shaik S, Schwarz H (2000) Acc Chem Res 33:139–145
25. Baciocchi EBM, Gerini MF, Lanzalunga O (2005) J Org Chem 70:5144
26. Guengerich FP, Yun CH, Macdonald TL (1996) J Biol Chem 271:27321–27329
27. Jurva U, Bissel P, Isin EM, Igarashi K, Kuttab S, Castagnoli N (2005) J Am Chem Soc 127:12368–12377
28. Li CS, Wu W, Kumar D, Shaik S (2006) J Am Chem Soc 128:394–395
29. Chen H, de Groot MJ, Vermeulen NPE, Hanzlik RP (1997) J Org Chem 62:8227–8230
30. Chen ZQ, Kang Y, Zhang CH, Tao J, Xue Y (2015) Theor Chem Acc 134:110
31. Shaik S, Cohen S, Wang Y, Chen H, Kumar D, Thiel W (2010) Chem Rev 110:949–1017
32. Sansen S, Yano JK, Reynald RL, Schoch GA, Griffin KJ, Stout CD, Johnson EF (2007) J Biol Chem 282:14348–14355
33. Tao J, Kang Y, Xue ZY, Wang YT, Zhang Y, Chen Q, Chen ZQ, Xue Y (2015) J Mol Graph Model 61:123–132
34. Kwiecien RA, Molinié R, Paneth P, Silvestre V, Lebreton J, Robins RJ (2011) Arch Biochem Biophys 510:35–41
35. Li DM, Wang Y, Yang CL, Han KL (2009) Dalton Trans 14:291–297
36. Schyman PUD, Wang Y, Shaik S (2010) J Phys Chem B 114:7078–7089
37. Kang Y, Tao J, Xue ZY, Zhang Y, Chen ZQ, Xue Y (2016) Tetrahedron 72:2858–2867
38. Zhang Q, Bell R, Truong TN (1995) J Phys Chem 99:592–599
39. Reed AE, Schleyer PR (1990) J Am Chem Soc 112:1434–1445
40. Mennucci B (2012) WIREs Comput Mol Sci 2:386–404
41. Schutz CN, Warshel A (2001) Proteins 44:400–417
42. Frisch MJ, Trucks GW, Schlegel HB, Scuseria GE, Robb MA, Cheeseman JR, Scalmani G, Barone V, Mennucci B, Petersson GA, Nakatsuji H, Caricato M, Li X, Hratchian HP, Izmaylov AF, Bloino J, Zheng G, Sonnenberg JL, Hada M, Ehara M, Toyota K, Fukuda R, Hasegawa J, Ishida M, Nakajima T, Honda Y, Kitao O, Nakai H, Vreven T, Montgomery JJA, Peralta JE, Ogliaro F, Bearpark M, Heyd JJ, Brothers E, Kudin KN, Staroverov VN, Kobayashi R, Normand J, Raghavachari K, Rendell A, Burant JC, Iyengar SS, Tomasi J, Cossi M, Rega N, Millam NJ, Klene M, Knox JE, Cross JB, Bakken V, Adamo C, Jaramillo J, Gomperts R, Stratmann RE, Yazyev O, Austin AJ, Cammi R, Pomelli C, Ochterski JW, Martin RL, Morokuma K, Zakrzewski VG, Voth GA, Salvador P, Dannenberg JJ, Dapprich S, Daniels AD, Farkas O, Foresman JB, Ortiz JV, Cioslowski J, Fox DJ (2013) Gaussian 09 revision D01. Gaussian Inc, Wallingford
43. Bach RD, Dmitrenko O (2003) J Phys Chem B 107:12851–12861
44. Wang Y, Kumar D, Yang CL, Han KL, Shaik S (2007) J Phys Chem B 111:7700–7710